Remote Sensing of Environment 113 (2009) 998–1011

Contents lists available at ScienceDirect

Remote Sensing of Environment

journal homepage: www.elsevier.com/locate/rse

# A simple band ratio technique to quantify the colored dissolved and detrital organic material from ocean color remotely sensed data

André Morel *, Bernard Gentili

*Laboratoire d'Océanographie de Villefranche (LOV), Université P.&M. Curie, et Centre National de la Recherche Scientifique, 06238 Villefranche-sur-mer, France*

ARTICLE INFO

*Article history:*
Received 23 October 2008
Received in revised form 14 January 2009
Accepted 17 January 2009

*Keywords:*
Remote sensing
Ocean color
Yellow substance detection
Yellow substance distribution
Corrected chlorophyll

ABSTRACT

Spectral reflectances of the ocean, $R$, as derived from ocean color remote sensing data at four wavelengths (412, 443, 490, and 555 nm), can be used to form two ratios of spectral reflectance, namely $R(412)/R(443)$, and $R(490)/R(555)$, thereafter denoted $\mathbf{R}_{443}^{412}$ and $\mathbf{R}_{555}^{490}$. The former is mainly sensitive to the colored dissolved organic material (CDOM), albeit influenced by the algal content as depicted by the chlorophyll concentration, ([Chl]); in contrast, the latter is essentially depending on [Chl], although it is also influenced by CDOM. Therefore the signatures of CDOM and [Chl] which are not truly separable, can nevertheless be identified by considering simultaneously the two ratios. The concomitant variations in these ratios can be established via a bio-optical model developed for Case 1 waters. This model implicitly includes a "mean" relationship between CDOM and [Chl], and thus produces a unique curve relating $\mathbf{R}_{443}^{412}$ to $\mathbf{R}_{555}^{490}$. Deviations with respect to this mean relationship can be introduced through a factor $\Phi$, with $\Phi>1$ (excess) or $<1$ (deficit), applied to the CDOM–[Chl] ratio. A family of $\mathbf{R}_{443}^{412}$–$\mathbf{R}_{555}^{490}$ curves is thus generated, in correspondence with the discrete values given to $\Phi$; this "grid" (or numerically, a 2-D lookup table) allows the $\Phi$–[Chl] couple to be unambiguously derived for any $\mathbf{R}_{443}^{412}$–$\mathbf{R}_{555}^{490}$ couple. By applying this straightforward algorithm to actual reflectance ratios derived from ocean color imagery, the relative anomalies in CDOM with respect to its standard (Chl-related) values can be efficiently assessed. Within the global ocean (discarding the coastal zones), the $\Phi$ factor is widely varying, between at least  and 3, and is roughly log-normally distributed around ~1 (no anomaly). The spatial distributions of the $\Phi$ factor in the whole ocean are strongly featured according to latitude, season, and hydrographic regimes, and these features are regularly reproducible, from year to year (2002–2007). This simple method is also validated against available in situ data, and its results compare favorably, for instance, to those of the GSM (Garver–Siegel–Maritorena) inversion method, in terms of retrieved CDOM concentrations and distribution patterns.



## 1. Introduction

Remote sensing of ocean color from space rests on the use of spectral channels providing radiometric information at a few selected wavelengths about the light backscattered from the upper layer of the ocean. Since the early stages of the ocean color history, and during the design of the first ocean color sensors, the implementation of a near-UV or a "violet" channel (in addition to other visible channels) has been envisaged. It was indeed argued at the Colloquium on "Passive Radiometry of the Ocean" (Patricia Bay, B.C., Canada, June 14 to 21, 1978) that such a violet channel could provide a path to discriminate between phytoplanktonic material and non-algal yellow substances (essentially dissolved yellow substance, or "gelbstoff", also denoted "CDOM", for chromophoric dissolved organic material). This Colloquium was held just before the launch of the CZCS sensor (see acronyms in Appendix A), so that the resulting recommendations (Morel & Gordon, 1980) for considering the benefits of a short-wavelength band were not intended for the CZCS, deprived from such a band; rather they were meant for future ocean color sensors. Actually, most of the sensors of the next generation were provided with a channel at 412 nm (OCTS, SeaWiFS, MODIS, MERIS), or at neighboring wavelengths (MOS, GLI), with the declared goal of detecting, and ultimately quantifying, the CDOM concentration. Somewhat surprisingly, however, a dedicated algorithm making a specific use of this violet band has not been proposed nor operated for the CDOM assessment during the last 30 years.

Presently, the empirical algorithm routinely employed for processing SeaWiFS and MODIS data (OC4v4, OC3M; see O'Reilly et al., 1998, 2000), or the semi-analytical algorithm for MERIS (OC4Me; Morel et al., 2007c) are based on the successive use of several ratios of reflectances involving wavelengths between 443 and 560 nm; they, however, leave aside the 412 nm channel and do not attempt to retrieve CDOM. The radiometric information from this 412 channel is yet combined with that of all other visible channels in various inversion techniques (e.g. Hoge & Lyon, 1996; Carder et al., 1999;

* Corresponding author.
*E-mail address:* morel@obs-vlfr.fr (A. Morel).

0034-4257/$ – see front matter © 2009 Elsevier Inc. All rights reserved.
doi:10.1016/j.rse.2009.01.008

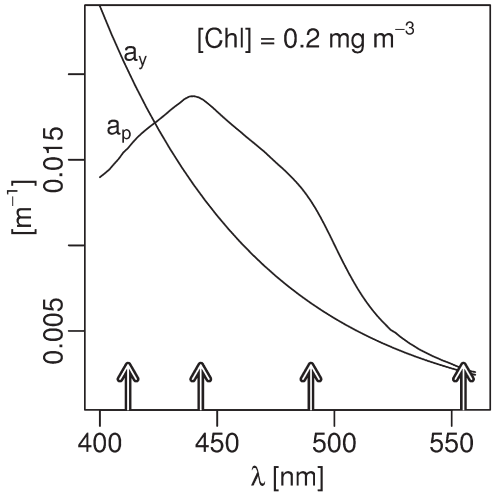


**Fig. 1.** Example of the spectral values of the yellow substance and particle absorption coefficients ($a_y$ and $a_p$, respectively) in Case 1 waters, when [Chl], the chlorophyll concentration, is equal to 0.2 mg m$^{-3}$ (a mean value for the global ocean). These average spectra are derived from empirical relationships for $a_p(\lambda)$ and $a_y(\lambda)$ (Bricaud et al., 1998; Morel, in press, respectively). The wavelengths involved in the present study are indicated by arrows.

Maritorena et al., 2002; Lee et al., 2002; Schiller & Doerffer, 2005; Smyth et al., 2006), or in the analysis of second order variability in satellite ocean color data (Brown et al., 2008). These inversion and semi-analytical techniques (see review in IOCCG, 2006) aim at simultaneously retrieving several inherent optical properties (such as particle backscattering and total absorption), and, for some of them, at separately assessing the partial absorptions due to CDOM and phytoplankton, respectively.

The initial proposition to dispose of and utilize a violet channel (cf. Fig. 4 in Morel, 1980) simply consisted of considering a 400 nm waveband in conjunction with 440 nm. As shown in Fig. 1, these wavelengths are those where the maximal absorption by yellow substance (at 400 nm) and by algae (at ~440 nm) are found within the visible spectrum. In addition, the slopes of opposite sign in the 400 to 440 nm domain of the absorption spectra by CDOM (decreasing) and by phytoplankton (increasing), a priori offer a possibility of discrimination that could be exploited. To a first approximation, the spectral irradiance reflectance, $R(\lambda)$ (the ratio of upward to downward irradiance, just beneath the surface; see Appendix B for definitions), is inversely proportional to the absorption coefficient, $a(\lambda)$. Therefore, the ratio of two reflectances, such as $R(400)/R(440)$, is mainly governed by the inverse ratio of the absorptions, $a(440)/a(400)$, so that a reduced $R(400)/R(440)$ ratio may denote an enhanced influence of CDOM.

Actually the situation is more complex, as this $R(400)/R(440)$ ratio is also sensitive to phytoplankton because their absorption is significant at both these wavelengths. In other words, the signatures of CDOM and algae are not separable, and it is thus necessary to get another piece of information, preferably more specific for the algal presence. Such an information is available when considering another waveband couple, as for instance 490 and 560 nm, particularly sensitive to phytoplankton pigments, and thus by forming the "blue-to-green" ratio, $R(490)/R(560)$. Although the CDOM absorption is notably diminishing at these longer wavelengths, its influence on this ratio is not negligible. In summary, as there is no possibility of fully isolating the influence of the two components, there is a need to simultaneously consider and combine in some way two ratios of reflectances, one more sensitive to CDOM, the other one more sensitive to pigments. It was the essence of the proposition made in 1980, and remains the rationale for the present feasibility study, essentially of methodological nature. Its aim is to re-examine the potentiality of such a simple method to disentangle the CDOM effect from intermingled signals.

The focus will be put on the CDOM content in Case 1 waters, which are defined as those oceanic waters outside of significant terrigeneous influences, and whose optical properties are chiefly determined by endogenous materials created through the biological activity. In such waters, the colored dissolved material is thus assumed to have been generated by algae and their degradation products. Nonetheless, the time and space scales involved in the generation processes, as well as in the subsequent decay processes, may (and generally do) result in an uncoupling between local CDOM and contemporaneous algal biomass (e.g., Bricaud et al., 1981). The simultaneous assessment of both components will allow the possible variations in the local CDOM-to-phytoplankton proportions to be detected and documented, which is an important piece of information in the description of the oceanic carbon cycle.

## 2. Modeling approach

### 2.1. The average situation regarding the CDOM–[Chl] proportions

The phytoplankton content in a water body is commonly described by the chlorophyll concentration, [Chl] (mg m$^{-3}$), and the CDOM component is generally quantified through its absorption coefficient (m$^{-1}$) at a specified wavelength, in the blue or violet part of the spectrum. Within the Case 1 water conceptual frame, CDOM and [Chl] are in principle co-varying. This entails that, at least, a certain "mean" relationship must exist between the two quantities. Actually, such a mean relationship can be derived from the empirical relationships describing the bio-optical properties of Case 1 waters (Morel, in press). At $\lambda = 400$ nm, for instance, the CDOM absorption coefficient, denoted $a_y$, has been found on average to increase with increasing [Chl] in a non-linear manner, according to

$$a_y(400, [\mathrm{Chl}]) = 0.065[\mathrm{Chl}]^{0.63} \quad (1)$$

Variability around this average relationship does exist in natural environment, and will be the main topic of the present paper. The spectral dependency of the CDOM absorption (cf. Fig. 1) is generally expressed through an exponentially decreasing function of the wavelength, λ, according to

$$a_y(\lambda, [\mathrm{Chl}]) = a_y(\lambda_0, [\mathrm{Chl}])exp[-S(\lambda - \lambda_0)] \quad (2)$$

where $\lambda_0$ is a reference wavelength and $S$ (nm$^{-1}$) is the slope of the exponential decay within the spectral range considered.

The influence of the CDOM content on the spectral reflectance, has to be estimated. The semi-analytical irradiance reflectance model, described in Morel and Maritorena (2001, thereafter denoted MM-01), however, does not explicitly include this particular absorbing component, nor its spectral behavior. Indeed, this model is initially based on the bulk diffuse attenuation coefficient for downward irradiance, $K_d(\lambda)$. It was empirically shown (Morel, 1988) that on average this coefficient depends on [Chl] in Case 1 waters, according to

$$K_d(\lambda) = K_w(\lambda) + \chi(\lambda)[\mathrm{Chl}]^{e(\lambda)} \quad (3)$$

The term $K_w(\lambda)$ corresponds to the contribution of pure water to $K_d(\lambda)$; the coefficient and exponent, $\chi(\lambda)$ and $e(\lambda)$, respectively, were obtained through regression analyses performed on the $[K_d(\lambda) - K_w(\lambda)]$ and [Chl] quantities determined in Case 1 waters. The $K_d(\lambda)$ coefficients, that are measured in situ, cumulate the effects of all absorbing (particulate and dissolved) components present in the water body. When building the MM-01 reflectance model, the $K_d(\lambda)$ coefficients are iteratively transformed into total absorption coefficients, $a_{tot}(\lambda)$. Therefore, these resulting absorption coefficients, like

$K_d(\lambda)$, account for the CDOM presence, and implicitly include the mean relationship as expressed by Eq. (1) (and related relations for other wavelengths — see below Eqs. (4a)–(4d).

The wavebands used in what follows slightly differ from those envisaged in 1980, and are selected because of their availability on modern sensors (namely 412, 443, 490, and 555 nm). The shortest available wavelength is 412 nm (not 400 nm), and the couple 490–555 nm will be considered (instead of 440–560). By using the MM-01 model (with the slightly revised $\chi(\lambda)$ and $e(\lambda)$ values from Morel et al., 2007c), the spectral reflectance and the needed ratios, $R(412)/R(443)$ and $R(490)/R(555)$, can be computed as a function of [Chl]; they are thereafter denoted $\mathbf{R}_{443}^{412}$ and $\mathbf{R}_{555}^{490}$. The $\mathbf{R}_{555}^{490}$ ratio decreases when [Chl] increases, and can be seen as a proxy of [Chl] in Case 1 waters. Indeed, it is one of the ratio routinely used in the maximum band ratio technique to retrieve [Chl] (e.g., see O'Reilly et al., 1998). As such, itessentially depends on [Chl], while it is still affected by changes in the CDOM relative concentration, but in a minimal way, to the extent that the CDOM absorption strongly weakens at 490 and 555 nm. On the contrary, $\mathbf{R}_{443}^{412}$ is very sensitive to CDOM and therefore to any change in the CDOM-algal proportions. In summary, for a given $\mathbf{R}_{555}^{490}$ value, i.e., for a given [Chl] value, the $\mathbf{R}_{443}^{412}$ ratio will decrease (increase) if CDOM absorption is above (below) its average value, as prescribed by Eq. (1). The theoretical $\mathbf{R}_{443}^{412}$ ratio is plotted as a function of $\mathbf{R}_{555}^{490}$ in Fig. 2a; both ratios are produced through the MM-01 model when [Chl] varies between 0.03 (tentatively 0.01) and 10 mg $m^{-3}$. This curve (annotated "mean") corresponds to the "standard" situation in terms of CDOM–[Chl] relative proportions, and as such agrees with, and implicitly includes, Eq. (1) (and Eqs. (4)–(4d), see later). It is worth noting that the portion of the curve for [Chl] <0.03 mg $m^{-3}$, which results from extrapolating the MM-01 reflectance model beyond its domain of strict applicability, is uncertain.

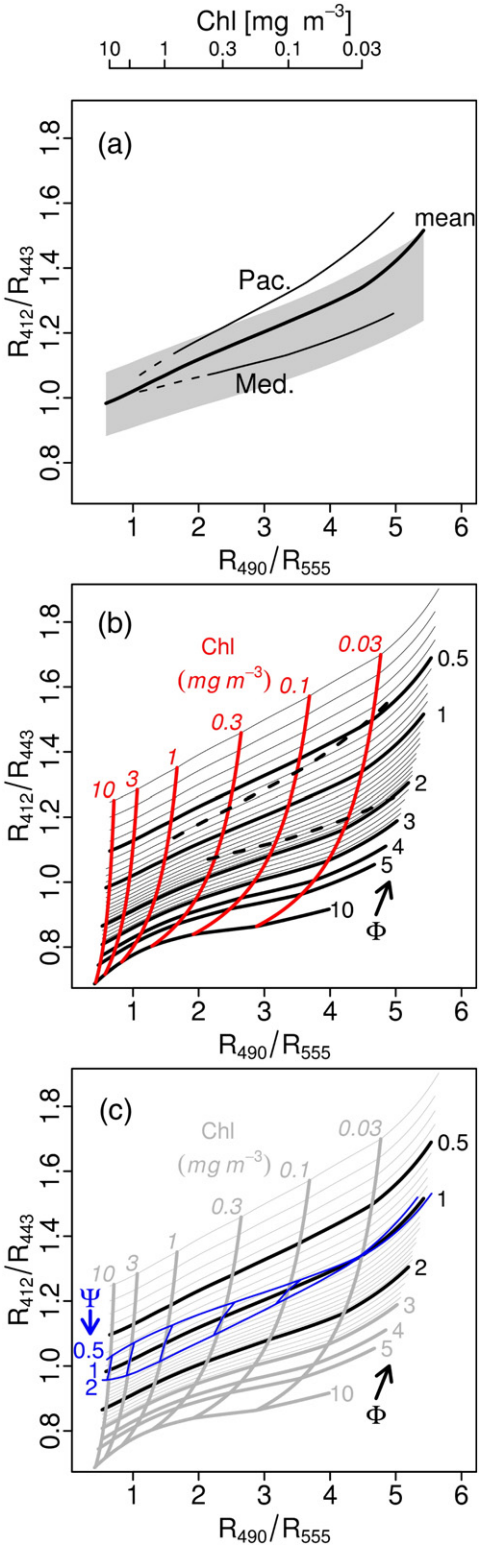


**Fig. 2.** a) Plot of $\mathbf{R}_{443}^{412}$ as a function of $\mathbf{R}_{555}^{490}$; the curve denoted "mean" represents the standard relationship between these ratios for Case 1 waters and when $S = 0.018\ nm^{-1}$ (Eq. (2)). The curves denoted "Med" and "Pac" represent specific relationships between the same ratios established for the Mediterranean and South-Eastern Pacific areas (see text). Secondary abcissae scale provides the [Chl] values, valid for the mean curve only. The Med. and Pac solid curves are limited to the [Chl] values encountered in these areas (solid lines becoming dashed lines). The shadowed stripe shows the Case 1 water "domain", as delimited by the inequalities proposed by Lee and Hu (2006) (see Eqs. (9) and (10)), with $\gamma = 0.1$. The ratios of remote sensing reflectances developed by Lee and Hu (their Eq. (2a)) must be transformed into ratios of irradiance reflectance (see Appendix B) to be represented on this plot. b) The mean curve ($\Phi = 1$) is reproduced from the previous panel in the same $\mathbf{R}_{443}^{412}$–$\mathbf{R}_{555}^{490}$ plane. Also displayed, the family of curves generated when the parameter $\Phi$ (cf. Eqs. (4)–(4d)) is introduced to modulate the CDOM content around its standard value. The increment in $\Phi$ between the isopleths is 0.1, when $0.5 < \Phi < 2$, then 0.2 when $\Phi$ is between 2 and 3. The isopleths corresponding to constant [Chl] values as indicated are shown in red. The dashed curves represent the Pacific and Mediterranean relationships reproduced from the panel a. c) The black curves for $\Phi = 0.5$ and 2 are reproduced from (b); the central curve is for $\Phi = \Psi = 1$, where $\Psi$ (see text) is the factor modifying the backscattering coefficient with respect to its nominal value; the blue curves are for $\Psi = 0.5$ and 2, as indicated. They cross each other when [Chl] is ~0.03 mg $m^{-3}$, as a result of the numerical parameterization, with no particular physical meaning (apart from being a consequence of the increasing importance of pure water backscattering compared to that of particles).

### 2.2. Variability in the CDOM–[Chl] proportions

Examples of such a variability in Case 1 waters, actually instances of systematic deviations with respect to the average law, were recently presented (Morel et al., 2007b). For a given [Chl] level in the Mediterranean Sea, the dissolved colored substance content appears to be systematically above the mean value derived for the global ocean. The converse is observed in South Pacific, particularly within the oligotrophic sub-tropical gyre, where the CDOM levels are lower than those expected from the mean relationship. These systematic (positive or negative) divergences in terms of $K_d$, are steadily and exponentially increasing when progressing into the UV domain, which undoubtedly authenticates the role of CDOM (or similar substances) in the observed process (Morel et al., 2007a; Morel et al., 2007b). These divergences, still notable in the blue-to-violet part of the spectrum, essentially vanishes beyond 500 nm. By accounting for these systematic differences, separate regressions analyses were made for the two water bodies (Fig. 3 in Morel et al., 2007a); they led to two

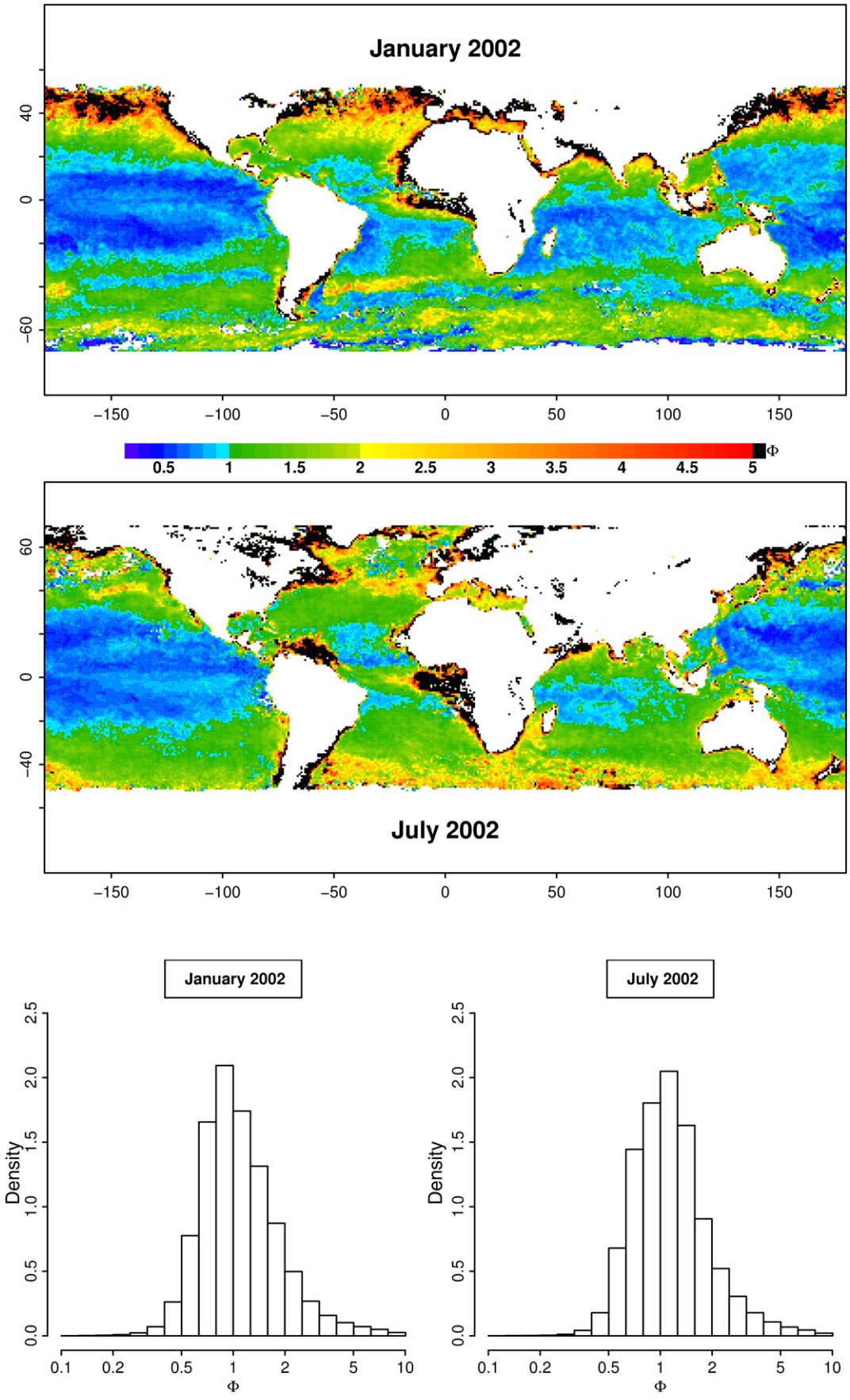


**Fig. 3.** Monthly composite from SeaWiFS (January and July, year 2002; 4320×2160 pixels, standard mapped image) processed in terms of CDOM anomaly, as quantified by the $\Phi$ index, according to the color encoding. The associated histograms are also displayed. The probability density are computed for the areas (i.e. the number of pixels combined with their area varying with the latitude). Before producing the $\Phi$ index, the "turbid flag" (Morel & Bélanger, 2006) is applied and eliminate the pixels corresponding to turbid Case 2 waters (mostly along the coasts).

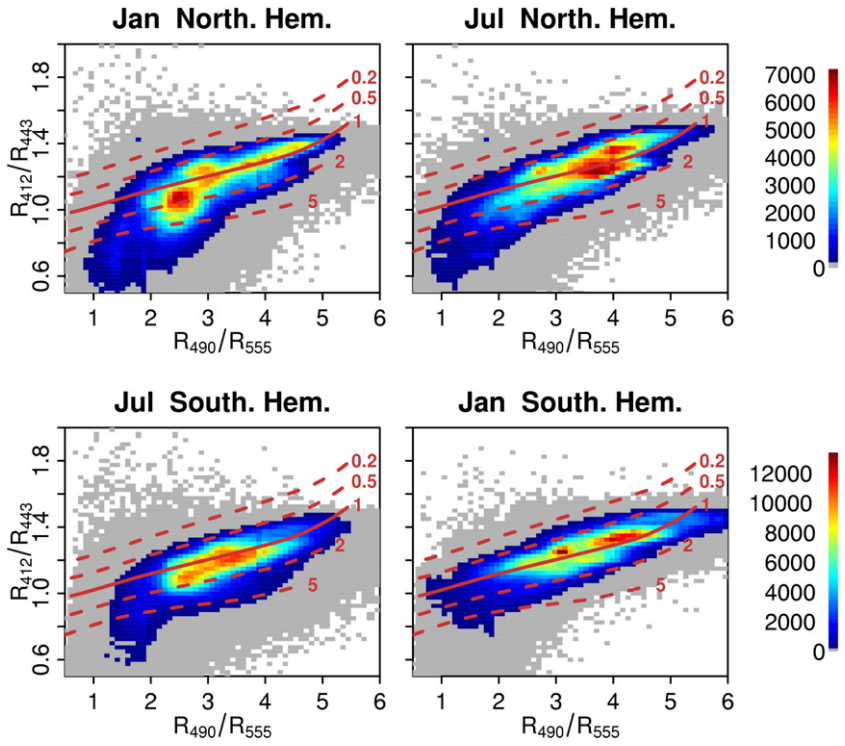


**Fig. 4.** Probability density (color scale) of the SeaWiFS data (2002) computed for two seasons and in each hemisphere, plotted within the $\mathbf{R}_{443}^{412}$–$\mathbf{R}_{555}^{490}$ plane (left column: winter; right column: summer). The total numbers of pixels represented are about 1.5 $10^6$ and 2.5 $10^6$ for the Northern and Southern hemispheres, respectively. The curves (simplified version of Fig. 2b) correspond to $\Phi = 0.5$, 0, 1, 2, and 4, as indicated.

specific sets of $\chi(\lambda)$ and $e(\lambda)$ values to express the links between the $K_d(\lambda)$ values and [Chl]. The same MM-01 reflectance model can be modified, namely operated with these particular, geographically distinct, $K_d(\lambda)$ values. The resulting $\mathbf{R}_{555}^{490}$–$\mathbf{R}_{443}^{412}$ relationships for the Mediterranean and Pacific zones differ from the average one, and are separately displayed on Fig. 2a. These differing relationships are typical examples of the variability possibly encountered in natural Case 1 water environments.

### 2.3. Quantification of the variability

A quantitative way of analytically showing the modifications in the $\mathbf{R}_{555}^{490}$–$\mathbf{R}_{443}^{412}$ relationship when the CDOM–[Chl] proportions change, consists of imposing deviations from Eq. (1), by introducing a factor $\Phi$, larger or lesser than unity, such as

$$a_y(400, [\mathrm{Chl}]) = \Phi 0.065 [\mathrm{Chl}]^{0.63} \quad (4)$$

by this way, $\Phi$ quantifies a relative departure (either an excess or a deficit) with respect to the standard Chl-dependent CDOM content. By using $S = 0.018$ nm$^{-1}$ in Eq. (2), the $a_y$ values for the other wavelengths of interest are

$$a_y(412, [\mathrm{Chl}]) = \Phi 0.0524 [\mathrm{Chl}]^{0.63} \quad (4a)$$

$$a_y(440, [\mathrm{Chl}]) = \Phi 0.0316 [\mathrm{Chl}]^{0.63} \quad (4b)$$

$$a_y(490, [\mathrm{Chl}]) = \Phi 0.0129 [\mathrm{Chl}]^{0.63} \quad (4c)$$

$$a_y(555, [\mathrm{Chl}]) = \Phi 0.0040 [\mathrm{Chl}]^{0.63} \quad (4d)$$

The $a_{tot}(\lambda)$ coefficients which were derived from the mean $K_d(\lambda)$ coefficients (see above) can now be modified by accounting for these changes imposed to the $a_y(\lambda)$ component when the factor $\Phi$ is varied. By operating the same reflectance model with these modified (either increased or decreased) $a_{tot}(\lambda)$ values as inputs, new reflectances are produced, forming a family of $\mathbf{R}_{555}^{490}$ vs. $\mathbf{R}_{443}^{412}$ curves, each of them corresponding to a given value of $\Phi$ (Fig. 2b). The isopleths corresponding to constant [Chl] values, together with the $\Phi$-isopleths, form a "grid" similar to that one which was displayed in Fig. 4 of Morel (1980).

By comparing the Mediterranean and the South-East Pacific curves of Fig. 2a and the family of curves of Fig. 2b, it appears that $\Phi$ would amount to about 1.5–2, in the Mediterranean Sea; the local CDOM content is thus about twice the oceanic average. In contrast, $\Phi$ is <1 in South-East Pacific, and is as low as 0.5 when [Chl] is about 0.03 mg m$^{-3}$, which is equivalent to a halving of the CDOM content compared to the standard one. Such geographical divergences demonstrate that wide variations in both directions in the CDOM-to-[Chl] relative proportions may be encountered in waters, which unquestionably are Case 1 waters from a biogeochemical point of view.

## 3. Results

### 3.1. Application to satellite imagery

The required $\mathbf{R}_{555}^{490}$ and $\mathbf{R}_{443}^{412}$ ratios can be derived from the products routinely delivered by the cognizant Space Agencies operating space-borne ocean color sensors. These products are generally provided for each waveband in terms of normalized water-leaving radiances, $nL_w(\lambda)$, or of remote sensing reflectance, $R_{rs}(\lambda)$, (Eqs. (A1) and (A2)) in Appendix B). These radiometric quantities are "exactly" normalized (superscript "ex"); in other words, they are corrected for bi-directional effects (depending on solar angle and viewing angle). They must be transformed into irradiance reflectance, $R$, and more specifically into $R_0$, that is the particular value of $R$ when the sun-zenith angle is nil (Eq. (A3)). After this simple transformation is achieved for each waveband, the resulting $\mathbf{R}_{555}^{490}$ and $\mathbf{R}_{443}^{412}$ ratios (Eqs. (A5) and (A6)) are introduced into the grid of Fig. 2b; actually they are

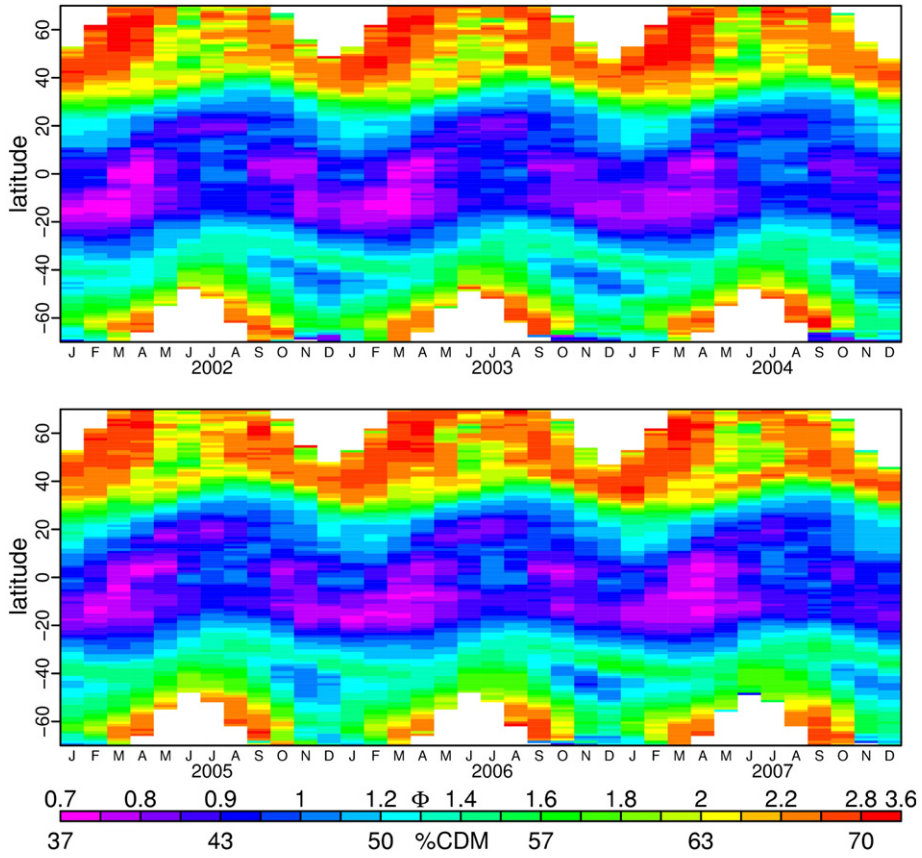


**Fig. 5.** Time-latitude (resolution: 1 month — 1° lat) distribution of the index $\Phi$ (zonal mean) for the years 2002 to 2007. Eq. (7) is used to establish the correspondence between the $\Phi$ scale and the %CDM scale to facilitate the comparison with Fig. 4 in Siegel et al. (2002).

interpolated into the corresponding lookup table (address in Appendix B) to get the appropriate $\Phi$ value.

Such a treatment has been systematically applied to SeaWiFS monthly global composites for the 2002–2007 period. Two instances at opposite seasons (January and July, 2002) are displayed in Fig. 3, together with the corresponding histograms showing the frequency of occurrence of the inferred $\Phi$ values. The first observation is that the $\Phi$ factor span a wide range, from about  to more than 3. The mode of the frequency distributions approximately coincides with $\Phi \sim 1$. As for the geographical patterns, below-the-mean CDOM proportions are typical of the subtropical oligotrophic gyres; these permanent deficits are particularly extended within the Pacific ocean. "Normal" values, or slight excesses (with $\Phi \sim 1$–1.5), are mainly encountered in the temperate latitudes in both hemispheres. More pronounced excesses (with $\Phi \sim 2$ or more) are essentially confined to high latitudes (40° and beyond), especially in the Northern hemisphere, where the highest $\Phi$ values are observed.

Not surprisingly, very high $\Phi$ values occur, more or less permanently, in zones under the influence of riverine discharges, actually within Case 2 waters, as for instance near the mouths of major rivers (Mississippi, Amazon-Orinoco, Rio de la Plata, Congo rivers, etc.), or in semi-enclosed seas and shallow waters (e.g., the Sea of Okhotsk, the Yellow Sea, the Argentinean shelf, the Persian Gulf, etc.); extremely high values are detected in the Black Sea and Baltic Sea, for instance, with $\mathbf{R}_{443}^{412}$ values occasionally outside of the grid of Fig. 2.

Opposite seasonal evolutions of the departures in each hemisphere tend to compensate with the result of smoothing the trends at global scale. Separate density plots are thus built for the two hemispheres and for the opposite months of July and January (Fig. 4). These density plots are overlaid onto a simplified version of the grid of Fig. 2b, so that the number of pixels (via the color encoding) with given $\Phi$ values can be directly visualized.

During the boreal winter in the Northern hemisphere (January), the highest density of pixels occurs for $\Phi = \sim 2$, with corresponding [Chl] values around 0.3 mg $m^{-3}$ (see [Chl] scales in Fig. 2). There is also a clustering (a tail) along the curve representing the standard CDOM proportion ($\Phi \sim 1$) for decreasing [Chl]. In austral winter (July) for the Southern hemisphere, a similar CDOM "excess" also occurs, although less accentuated ($\Phi$ slightly above 1). In summertime for both hemispheres, the situation drastically changes. The CDOM excesses almost disappear in the Northern hemisphere, whereas in the Southern hemisphere, they are even replaced by slight deficits. This summer decrease in CDOM relative contents is systematic, and very likely has to be attributed to the effect of a generalized photo-bleaching process (Nelson et al., 1998). For the contrasted zones already mentioned (the Mediterranean Sea, and the South-eastern Pacific), the same shift between winter and summer $\Phi$ values is observed despite the very differing background values (see later Fig. 6d). The $\Phi$ values are displayed in Fig. 5 as a function of latitude and months for the 2002–2007 period. These zonal distributions confirm and generalize the comments previously made from the results shown in Fig. 4. The marked N–S dissymmetry of the high latitudes (excesses more extended in the Northern hemisphere), the seasonal N–S migration of the subtropical areas exhibiting deficits, which actually follows the sun declination (with a small, 1–2 months, time lag) and thus supports the hypothesis of a photo-bleaching effect, all these phenomena are repeatedly observed with the present method; they were already observed by using the "GSM" method (see below), as illustrated by Fig. 4 in Siegel et al. (2002).

The probability of occurrence of the $\Phi$ values (Figs. 3 and 6a,b) is approximately distributed according to a log-normal law for the global ocean and the entire year. The mode roughly coincides with the CDOM standard value ($\Phi \sim 1$). About 80% of the observations fall between half or twice this value (i.e., $\Phi$ between 0.5 and 2). Such a distribution is

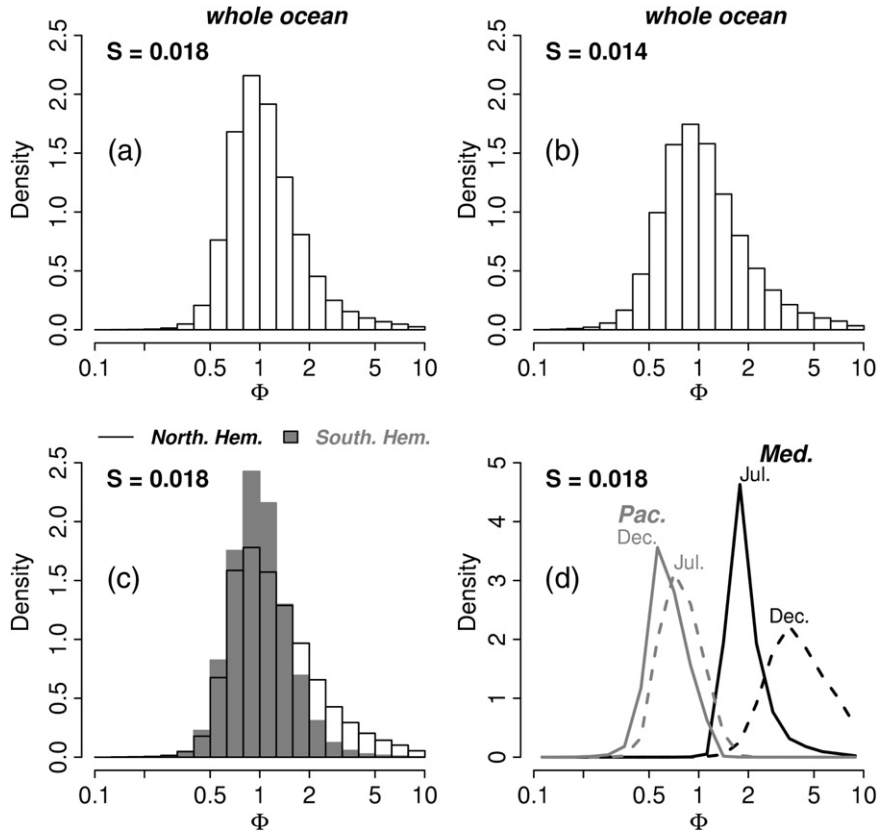


**Fig. 6.** Probability density distributions of the $\Phi$ values (SeaWiFS data; year 2006). a) for the global ocean and over the whole year, when the slope $S$ (Eq. (2)) is set equal to 0.018 $nm^{-1}$; b) as in (a), except for $S = 0.014$ $nm^{-1}$. c) overlaid histograms for the Northern Southern hemispheres (open and shaded histograms, respectively); d) Separate histograms for two opposite seasons and for two specific zones; the South Pacific sub-tropical gyre (delimited by 110–140°W, 27–15° S) that permanently shows marked deficits compared with standard content, and the entire Mediterranean Sea (Black Sea excluded); this sea shows permanent CDOM excesses (see also Morel, Claustre, et al., 2007). When $S = 0.018$ $nm^{-1}$ (a), 80% of the pixels occur when $\Phi$ is between 0.56 and 1.87; this interval becomes 0.48–2.14, when $S = 0.014$ $nm^{-1}$ (b).

also valid in the case of the Southern hemisphere (Fig. 6c), whereas for the Northern hemisphere the skewed shape of the histogram slightly differs from that of the log-normal distribution, with CDOM values above the standard ones more frequently represented.

A detailed description and interpretation of the geographical–temporal distribution of the $\Phi$ index within the world ocean is beyond the scope of the present paper, essentially devoted to methodology. Actually, a global distribution of the "colored dissolved and detrital organic materials" (denoted "CDM") has already been described by Siegel et al. (2002), Siegel, Maritorena, Nelson, and Behrenfeld (2005), Siegel, Maritorena, Nelson, Behrenfeld, and McClain (2005). It remains interesting, however, to compare Siegel et al.'s methodology with the present one, as well as the exact nature of the results they both provide.

### 3.2. Comparison with the GSM approach: absolute and relative estimates of CDM

The amount of CDM, defined in terms of an absorption coefficient, $a_{CDM}$ at $\lambda = 440$ nm, is a nominal product of the "GSM" semi-analytical inversion scheme applied to ocean color data. This inversion technique, initially developed by Garver and Siegel (1997) and updated by Maritorena et al. (2002) (hence the acronym GSM), was designed for use with SeaWiFS and MODIS data over non-coastal waters (same limitation as for the present approach). It has been implemented in SeaDAS, and is also systematically operated in the frame of the GlobColour Project (http://www.globcolour.info/) which produces global ocean color maps (level-3) by merging the data from the three sensors SeaWiFS, MODIS, and MERIS (see also Maritorena & Siegel, 2005).

According to its definition, the $a_{CDM}$ (440) coefficient includes the absorption by both the chromophoric dissolved organic matter (CDOM) and the detrital, actually the non-algal (colored) particulate matter (NAP). These two components are considered together because of the similar shape of their absorption spectra, and thus the difficulty in differentiating them in absence of a mechanical (namely a filtering) treatment. In contrast, a filtering technique is involved in the definition of CDOM. Indeed, this dissolved (plus colloidal) material is operationally and conventionally defined as the material able to pass through a membrane filter with 0.2 µm pore size (protocols in Mueller & Fargion, 2002).

Here (specifically in Eq. (1)), the absorption $a_y$ has been obtained as a difference $(a_{tot} - a_p)$ between the total absorption (derived by inversion) and the particulate absorption (measured according to the glass-fiber filter technique; Bricaud et al., 1998). For these $a_p$ measurements, the particulate matter was collected by using GFF filters, with an effective pore size of about 0.5 µm (nominally 0.7 µm); this threshold is not clearly defined because of progressive clogging. Therefore (discussion in Morel, in press), the absorption by some tiny particles in the 0.2–0.5 µm size range, not included in $a_p$, is in turn included in $a_y$. In total, $a_y$ might be larger than $a_{CDOM}$ but smaller than $a_{CDM}$. Between these three terms, however, the differences are likely minute insofar as the absorption by the dissolved component would dominate the NAP absorption (Siegel et al., 2002; see also Figs. 4 in Morel, in press).

Beside the real differences in methodology and algorithm between the GSM inversion and the present approach, an apparent difference lies in the way of expressing the results. The former provides an absolute magnitude of the CDM absorption ($a_{CDM}$ is expressed as $m^{-1}$), and its derivation is independent from the chlorophyll content. In contrast, the present approach provides a "relative" estimate, since it quantifies the

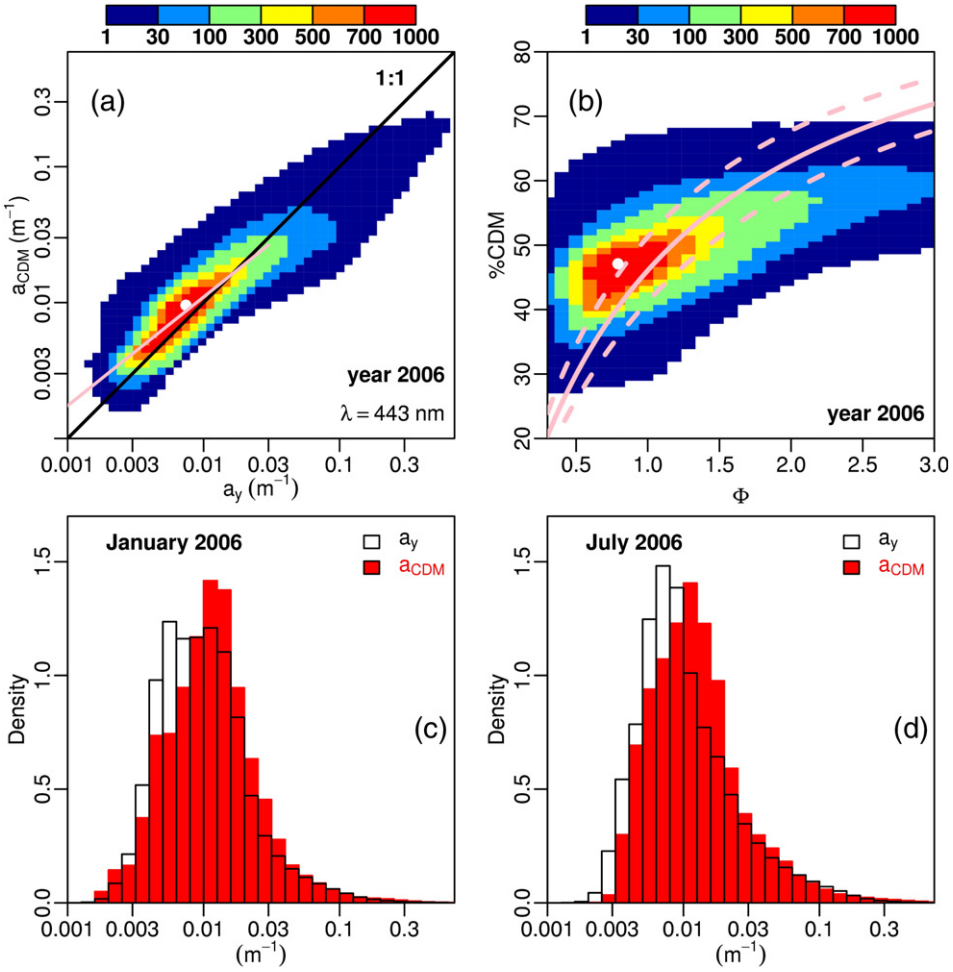


**Fig. 7.** Two-dimensional relative frequency distributions of pixels (color encoding); the white dot in each panel shows the position of the maximum. a) $a_{CDM}$ vs. $a_y$ plot (see text). The $a_{CDM}$ coefficient is provided by the GSM technique applied to the 12 monthly composites (year 2006) for the global ocean (GlobColour product); the 1:1 line is shown; the slope of the linear regression (pink line) between the $\log_{10}$-transform of the quantities amounts to 0.74 (with $r^2 = 0.79$, and RMSE = 0.132). b) From the same results as in panel a, comparison between the $\Phi$ index and the %CDM parameter. The solid pink curve corresponds to Eq. (7); the dashed curves correspond to a ±20% uncertainty in the phytoplankton absorption (Eq. (6)). c and d) Histograms of the distribution of the $a_y$ and $a_{cdm}$ values (m$^{-1}$) for the global ocean and the two months as indicated. In January, the median of the distributions are 0.0087 m$^{-1}$ for $a_y$ (3.46 10$^6$ pixels at the maximum), and 0.0099 m$^{-1}$ for $a_{CDM}$ (3.70 10$^6$ pixels at the maximum); in July, the corresponding numbers are 0.0083 and 0.100 m$^{-1}$ with 3.14 and 3.34 10$^6$ pixels, for $a_y$ and $a_{CDM}$, respectively.

actual CDOM content in reference to a "standard" content depending on [Chl] according to Eq. (1). The comparison between the products of the two methods can be performed either directly or indirectly.

The direct comparison consists of simultaneously using the [Chl] values and the estimated $\Phi$ factor to compute the actual $a_y$ (440) value (via Eq. (4b)), which is straightforwardly comparable to the GSM product, $a_{CDM}(440)$. This comparison is graphically presented on Fig. 7a. The number of data represented amounts to about $38 \times 10^6$, obtained by cumulating the pixels of the 12 global monthly composites for the year 2006. The agreement between the two quantities is very good; the $a_y$ values (particularly those below 0.02 m$^{-1}$) are slightly shifted toward smaller values when compared with the $a_{CDM}$ values, perhaps as a consequence of the inclusion into $a_{CDM}$ of the NAP absorption. If not perfectly coinciding, the histograms for $a_y$ and $a_{CDM}$ (Fig. 7c and d) are sufficiently close to demonstrate the overall agreement between the two distinct estimates; the medians of the $a_y$ distributions are smaller than those of $a_{CDM}$ by about 15% (see legend of Fig. 7c and d). With such small differences and similar geographical patterns, the $a_y$ and $a_{CDM}$ global maps (not shown) are hardly distinguishable.

The indirect comparison involves the relative estimates and establishes another link between the two approaches. Siegel et al. (2002), Siegel, Maritorena, Nelson, and Behrenfeld (2005), Siegel, Maritorena, Nelson, Behrenfeld, and McClain (2005) observed that the global patterns of CDM mimic the basin-scale chlorophyll distribution. Such a similarity implies that, to first order, CDM roughly co-varies with [Chl], and a significant correlation coefficient (0.751) was found by Siegel, Maritorena, Nelson, and Behrenfeld (2005, their Table 3). Their Fig. 3a confirms this covariation (incidentally, the trend in this figure agrees nicely with Eq. (4b), when $\Phi = 1$). Therefore, these authors introduced a relative estimate of CDM in reference to the [Chl] content, by computing a dimensionless quantity, denoted "percentage CDM" which is defined as

$$\%\mathrm{CDM} = (100) \cdot a_{CDM}(440) \,/\, \left[a_{CDM}(440) + a_{\varphi}(440)\right] \tag{5}$$

and represents the fractional non-water absorption due to CDM; $a_{\varphi}(440)$, that stands for the phytoplankton absorption at 440 nm, is adopted from Bricaud et al. (1998)

$$a_{\varphi}(440) = 0.03782[\mathrm{Chl}]^{0.635} \tag{6}$$

The variations in %CDM obviously bear some resemblance with $\Phi$, the relative departure from the average. The numerical relationship between these two quantities is particularly simple. By introducing the expressions (4b) and (6)s into Eq. (5), and noting that the

exponents (~0.63) practically coincide, the following hyperbolic relationship

$$\%\mathrm{CDM} \sim (100\%)0.032\Phi / [0.038 + 0.032\Phi] \quad (7)$$

is derived. Note that in absence of anomaly (i.e., when $\Phi = 1$), Eq. (7) leads to %CDM = 46%, a central value very close to those found as being the global oceanic mean values (namely 51% in Siegel et al., 2002, or 46% in Siegel, Maritorena, Nelson, & Behrenfeld, 2005). The %CDM values computed for the same data as in Fig. 7a are plotted as a function of the $\Phi$ values in Fig. 7b. The majority of the data are assembled along the central part of the curve representing Eq. (7). Despite a considerable scatter, the two parameters develop in the same way, apart from the saturating plateau for %CDM occurring when $\Phi$ exceeds 2 (Fig. 7b. The above relationship (Eq. (7)) has been used in Fig. 5 to convert the $\Phi$ scale into a %CDM scale.

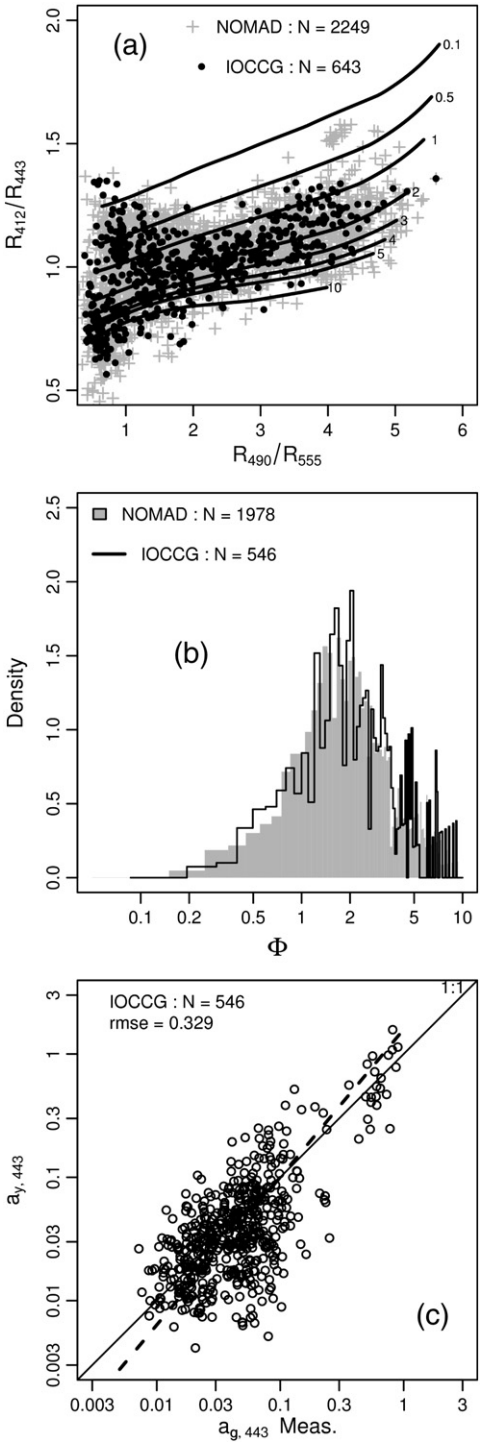


**Fig. 8.** a) Data (from both NOMAD data set and IOCCG data subset) plotted in the $\mathbf{R}^{412}_{443}$–$\mathbf{R}^{490}_{555}$plane. Note that many data with low $\mathbf{R}^{490}_{555}$ (corresponding to high [Chl]) are outside of the grid in both directions; these data will not provide a reliable $\Phi$ value and are not represented in (c); b) Corresponding histograms of the $\Phi$ index; c) retrieved $a_y$ absorption vs. field determinations, $a_g$ (NOMAD data). The solid line is the 1:1 line; Type II regression in log space (dashed line) provides for the slope, intercept, and $r^2$ the following values 1.131, 0.108, and 0.463, respectively. The number of data is reduced compared to those in (a), because of unrealistic $\Phi$ values.

### 3.3. Impact of varying CDOM-to-[Chl] proportions onto the [Chl] retrieval

Standard algorithms (e.g., OC4v4) used to retrieve [Chl] tacitly implies that the average CDOM-to-[Chl] proportions are respected. Undetected deviations from these proportions obviously translate into a bias in the [Chl] estimates. The importance of this bias can easily be inferred from Fig. 2b, by imagining an intersection between a vertical line and the curves forming the grid. To a given $\mathbf{R}^{490}_{555}$ value corresponds a certain [Chl] value on the curve for which $\Phi = 1$. If $\Phi$ differs from unity, differing [Chl] values will be derived since the isopleths for [Chl] are not vertical. It can easily be seen that when $\Phi < 1$, the [Chl] value (derived with $\Phi = 1$) is overestimated, and the converse holds true when $\Phi > 1$. A simple qualitative reasoning leads to the same conclusion (the missing absorption resulting from a deficit in CDOM is "compensated" via the nominal algorithm by an increase of the estimated [Chl], and vice-versa). The quantitative assessment of this effect can be made from the numerical data corresponding to the grid of Fig. 2b. The relative difference, ΔChl (%)

$$\Delta\mathrm{Chl} = 100[(\mathrm{Chl}_{\mathrm{act}} - \mathrm{Chl}_{\mathrm{ret}}) / \mathrm{Chl}_{\mathrm{act}}] \quad (8)$$

between the actual [$\mathrm{Chl}_{\mathrm{act}}$], and [$\mathrm{Chl}_{\mathrm{ret}}$], the concentration retrieved when the CDOM effect is ignored, is displayed on Fig. 9. This relative difference (or corrective term) depends on the parameter $\Phi$, and is positive when $\Phi < 1$ and negative when $\Phi > 1$. It is almost independent from the [Chl] value itself (at least when [Chl] < 1 mg $m^{-3}$), and may reach ±20% for the most frequently encountered $\Phi$ values (between 0.5 and 2). It is nearly independent from the hypothesis adopted for the slope $S$ (except for the very low $\Phi$ values).

The above analysis supports the results shown by Siegel, Maritorena, Nelson, Behrenfeld, and McClain (2005), in particular in their Fig. 1 where the discrepancies in the [Chl] assessment appear to be well correlated with the magnitude of the CDM absorption. It also supports old statements saying that a desirable accuracy in pigment retrievals of ±30% is reachable, but difficult to surpass because of natural limitations. The varying relative contribution of CDOM is one of the main causes, and probably the major one, of such limitations in Case 1 waters. Information contained in Fig. 9 can straightforwardly be used to correct a first estimate of [Chl] obtained through the standard algorithm, once the index $\Phi$ has been independently assessed (Fig. 10). Operating such a two-step procedure actually is a transparent way of repeating what is made through more complex inversion and optimization methods based on the same array of spectral quantities (cf. Introduction).

The problem of re-estimating [Chl] could also be handled somewhat differently. When a pixel, via its $\mathbf{R}^{412}_{443}$ and $\mathbf{R}^{490}_{555}$ ratios, is inserted into the grid of Fig. 2b (into the numerical 2-D lookup table; address in Appendix B), both quantities, $\Phi$ and [Chl], are simultaneously determined. Therefore, there is no longer a need to adjust the [Chl] estimate. A possible criticism for this approach is that in this case [Chl] is assessed through a single spectral ratio ($\mathbf{R}^{490}_{555}$), instead of using the MBR (maximum band ratio) technique, reputed to be more sensitive and accurate. As expected, only minute differences occur between the two [Chl] re-estimates in the middle [Chl] range (i.e., when the MBR and $\mathbf{R}^{490}_{555}$ coincide); notable differences, however, appear particularly at low [Chl] concentration.

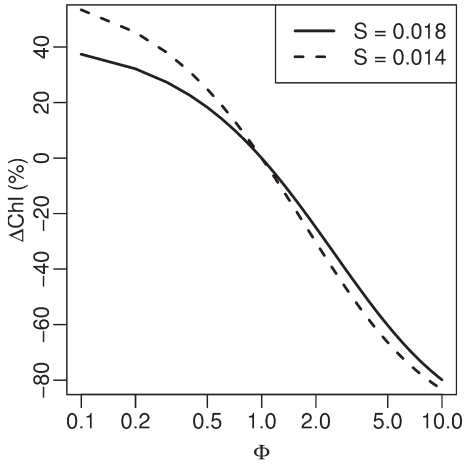


**Fig. 9.** Relative per-cent difference, ΔChl (%, Eq. (8)), between the actual [$Chl_{act}$] value and the retrieved value, [$Chl_{ret}$], as a function of the $\Phi$ index (log-scale), and for two values of the slope $S$, as indicated. For $S=0.018\ nm^{-1}$, the fit between $Y$ ($=\Delta Chl\ \%$) and $X$ ($=\log_{10}\Phi$) to a polynomial of the 4th order, $Y=\sum_{n=1}^{4} A_n X^n$, is obtained with the coefficients as follows $A_1=-73.65$, $A_2=-35.92$, $A_3=15.30$, $A_4=14.80$.

The use of classical MBR algorithms to derive [Chl], followed by a correction accounting for the CDOM variability based on an additional band ratio, is certainly the more robust and logical method. Instances of its application to the SeaWiFS data (January and July 2006) for the global ocean are provided under the form of histograms (Fig. 10), where the initial (OC4v4)-[Chl] retrieval, the corrected [Chl], and the "GSM"–[Chl] are displayed. The major impacts of the ΔChl correction are i) to reduce the number of pixels exhibiting [Chl] values exceeding 0.3 mg $m^{-3}$ range, when [Chl] was often overestimated in presence of positive CDOM anomalies ($\Phi>1$), and correlatively ii) to increase the number of pixels with [Chl] around 0.1 mg $m^{-3}$. Globally, the ΔChl correction results in a narrowing of the frequency distribution, which is also observed with the GSM–[Chl] values. The medians (see legend) are slightly shifted toward lower [Chl] values for the entire ocean. Locally, the effect of the correction may be more spectacular in zones where $\Phi$ differs markedly and permanently from 1 (e.g., in the Mediterranean Sea).

### 3.4. CDM variability within Case 1 waters (comparison with Lee and Hu approach)

Although it was imagined for another purpose, a method akin to the present one was presented by Lee and Hu (2006; thereafter denoted LH). Their aim was to identify what they called "exact" Case 1 waters; for that, they defined a criterion based on the importance of the non-algal absorption (actually the CDM absorption) relatively to the absorption which is normally associated with the [Chl] level. Turbid Case 2 waters (not discussed here) were also identified by LH through another criterion based on the backscattering excess.

The influence of CDM was quantified by the means of two ratios utilizing the same wavebands as here. These ratios slightly differ from those considered here, because they involve the remote sensing reflectance, $R_{rs}$, instead of the irradiance reflectance, $R$. For this reason, they will be denoted $\mathbf{R}^{412}_{443}$ and $\mathbf{R}^{490}_{555}$. The concomitant variations of these two ratios with [Chl] were modeled for Case 1 waters via the MM-01 reflectance model, resulting in a relationship (fitted to a 3rd order polynomial) similar to the "mean" curve in Fig. 2a, and simply summarized as

$$\mathbf{RS}^{412}_{443} = f\left(\mathbf{RS}^{490}_{555}\right) \tag{9}$$

When produced by this equation, the $\mathbf{R}^{412}_{443}$ value is written $R^{CS1}$, according to the notation adopted by LH, where the superscript (CS1) means "exact " Case 1 water. By inserting into Eq. (9) the actual $\mathbf{R}^{490}_{555}$ value as determined for a certain pixel (of an ocean color scene), this equation returns the $\mathbf{R}^{412}_{443}$ value for this pixel. This actual value is compared to the exact one (to $R^{CS1}$), and the comparison is performed through the successive inequalities

$$(1-\gamma)R^{CS1} < \text{actual } \mathbf{R}^{412}_{443} < (1+\gamma)R^{CS1} \tag{10}$$

This criterion, as defined by LH, has the following meaning: "Exact" Case 1 waters correspond to $\gamma=0$ (i.e., when $\mathbf{R}^{412}_{443}=R^{CS1}$); a pixel, however, can still be considered as belonging to Case 1 waters if the inequalities above are fulfilled. Somewhat arbitrarily, LH chose $\gamma=0.1$ to fix the lower and upper thresholds. This criterion is graphically represented in Fig. 2a, as the shaded stripe corresponding to $(1\pm\gamma)=0.9$ and 1.1.

By comparing this stripe with the grid in Fig. 2b, it can be seen that the lower limit adopted by LH (i.e., 0.9 $R^{CS1}$) roughly corresponds to a CDOM relative excess described by $\Phi\sim2$; their upper limit (1.1 $R^{CS1}$) corresponds to a relative deficit, with $\Phi\sim0.6$ when [Chl] is high, or even to "no anomaly" ($\Phi=1$), at low [Chl]. In reality, variations of much larger amplitudes than those adopted by LH can be observed in Case 1 waters, as demonstrated by the previous examples (Pacific, Mediterranean and global ocean waters). In particular, the LH upper limit does not allow for CDOM deficits at low [Chl] level, a situation

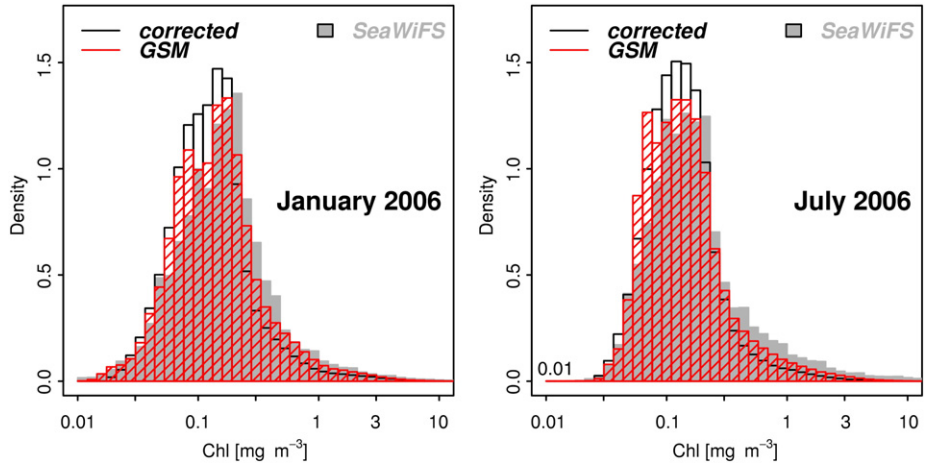


**Fig. 10.** Example of application of the ΔChl (Eq. (8)) correction to the SeaWiFS [Chl] values for the same monthly composites already used for Fig. 7. In January 2006, the median value shifts from 0.144 mg $m^{-3}$ (uncorrected OC4V4 — SeaWiFS data) to 0.112 mg $m^{-3}$ (after the ΔChl correction), and to 0.124 mg $m^{-3}$ for the GSM data; in July 2006, the median shifts from 0.138 to 0.115, and 0.117 mg $m^{-3}$, respectively.

which apparently is systematically encountered in most of the oligotrophic gyres (such as those in the Pacific Ocean — Fig. 3). The definition of "Case 1" waters can be seen as a rather semantic question, and their delimitations somewhat arbitrary; however, the rather restrictive criteria adopted by LH will be briefly discussed later on.

Note that Brown et al. (2008), after having removed the first order effects of [Chl] on ocean color signal, are able to identify a second order effect due to CDM variability, also via an anomaly in the ratio of the normalized water-leaving radiances at 412 and 488 nm. These anomalies actually represent the variability in the relative proportions of CDM to [Chl] that diverge from the mean trend (in a way differing from, albeit similar to, that adopted here with the deviation index $\Phi$). Like $\Phi$, these anomalies are widely varying in both directions (excess or deficit) in Case 1 waters within the world ocean.

## 4. Discussion

A preliminary remark is about the quality of the marine signal retrieved at 412 nm. Achieving accurate atmospheric corrections at this wavelength is known to be a difficult task. This problem is crucial in coastal zones, where the assessment of the aerosol content via the near-infra-red bands is questionable because of the interference with the local turbidity (i.e., when the "black pixel" assumption fails). Even if less acute, the problem is still posed in oceanic Case 1 waters presently under consideration, as the extrapolation of the aerosol signal captured in NIR is inevitably uncertain, and the inaccuracy of the atmospheric correction is growing for decreasing wavelengths (so that the 412 nm channel is the more affected one), and also growing with the air mass (with increasing sun and view angles). The examination of these well known difficulties is beyond the scope of the present study. They have to be kept in mind, however, particularly when critically assessing the capabilities offered by other spectral channels in the near UV, or at 400 nm, as often proposed for implementation into future sensors.

The following discussion is organized according to successive distinct points. The first point deals with some assumptions, not yet discussed, which involve the effect of backscattering. The second point presents a sensitivity study with respect to plausible hypotheses regarding the spectral shape of the CDOM absorption. A validation of the present method is then presented (3rd part) by comparison with available in situ data. Some considerations about the accuracy of the CDOM estimates are provided (4th part). Finally (5th part), and before concluding, the statistics of the CDOM deviations within Case 1 waters are briefly analyzed in relation to the extension of these waters.

1. The changes in the $\mathbf{R}_{443}^{412}$ and $\mathbf{R}_{555}^{490}$ ratios and modifications in their inter-relationship have only been attributed to the consequence of varying proportions between non-algal and algal absorption (for a given [Chl] value). Other causes are possible. Indeed, "non-standard" backscattering coefficients, $b_b(\lambda)$, can also produce little changes in the $\mathbf{R}_{443}^{412}$ and $\mathbf{R}_{555}^{490}$ ratios. This possibility, left aside in the present study, has a lesser impact, compared to the effects of varying absorption, as it is made clear with Fig. 2c. In a way similar to that employed when constructing Fig. 2b, a perturbation is introduced in the MM-01 model, by allowing the particulate backscattering coefficient to be halved or doubled with respect to its standard, Chl-dependent, value (Eqs. (12), (13), and (14) in MM-01). The perturbation is determined by a factor $\Psi = (0.5 \text{ or } 2)$, without specifying its cause; it may be caused by a change in the relationship between the particle scattering $b_p$ and [Chl], or by a change in the backscattering probability, $\tilde{b}_{bp}$. The spectral dependence of $b_p$ is left unchanged (Eq. (18) in Morel, in press). The effect of changing $\Psi$ upon the $\mathbf{R}_{443}^{412}$–$\mathbf{R}_{555}^{490}$ relationship is considerably reduced compared to that one resulting from a similar change in $\Phi$. In particular, the impact is practically negligible for most oceanic waters, when [Chl] is below 0.1 mg $m^{-3}$. Such a result is expected because in the blue part of the spectrum the contribution of water molecules (and ions) to the backscattering coefficient is dominant, (between 72% and 94% at 412 nm, when [Chl] goes from 0.5 to 0.03 mg $m^{-3}$; see Morel & Gentili, 1991), so that the role of $b_{bp}$ and of its variations is minimized. In Case 1 waters with higher [Chl] value, the effects of fluctuation in backscattering becomes notable, albeit less than those of CDOM deviations. These effects may, however, interfere with the estimate of the latter, by acting in the same direction, in such a way that an unidentified excess (reduction) of backscattering will be interpreted as an excess (deficit) in CDOM, at least when [Chl] exceeds 0.1 mg $m^{-3}$. The slight excess (Fig. 7a) of $a_y$ compared to $a_{CDM}$, observed when $a_y$ is high and exceeds 0.03 $m^{-1}$ (when [Chl]>1 mg $m^{-3}$), could result from an above average backscattering coefficient (beside the effect of colored particulate matter, already mentioned). Discriminating such a scattering impact from the absorption variability is not accessible to the simple method described here; for that, more sophisticated empirical approach (see e.g. Brown et al., 2008), or other inversion tools which, beside band ratios involve the absolute magnitude of reflectance (or of $nL_w$), are needed. Another type of variations in the $\mathbf{R}_{443}^{412}$ and $\mathbf{R}_{555}^{490}$ ratios, independent from CDOM and not accounted for, may originate from the variability in $a_p$, for a given [Chl] value (Bricaud et al., 1998). Such an undetected variability is by default transferred onto the CDOM (or CDM) estimates.
2. The development of the present tool rests on the grid displayed on Fig. 2b, the building of which has included a hypothesis about the slope of the exponential decay ($S$, in Eq. (2)). It is therefore important to examine how the estimate of the CDOM anomalies is sensitive to this parameter. If $S$, presently set equal to 0.018 $nm^{-1}$, is modified, the "mean" curve (for $\Phi = 1$) will obviously stay unaffected, as it derives from the MM-01 model where the implicit CDOM content does not intervene numerically. The slope value comes into play when departures from the standard CDOM content are modeled, more precisely when Eqs. (4a)–(4d) are derived from Eq. (4) in order to compute the modified $R(\lambda)$. The effect of changing $S$ can be easily imagined. The CDOM spectral absorption will be less steep if the $S$-value 0.018 $nm^{-1}$ is, for instance, replaced by a smaller value (such as 0.014 $nm^{-1}$). In this case, and for a given [Chl] value, the $\mathbf{R}_{443}^{412}$ and $\mathbf{R}_{555}^{490}$ ratios (particularly the first one, more sensitive to the CDOM content) become less dependent on the $\Phi$ value than they were when $S$ was 0.018 . As a consequence, the grid in Fig. 2b slightly shrinks, particularly along the vertical direction. When overlaid onto this new narrower grid (produced with $S = 0.014$ $nm^{-1}$), the $\mathbf{R}_{443}^{412}$ and $\mathbf{R}_{555}^{490}$ ratios extracted from an ocean color image, will lead to $\Phi$ values beyond those previously derived when the wider grid (built with $S = 0.018$ $m^{-1}$) was used. This extension toward extreme $\Phi$ values in both directions (excess and deficit), and correlatively the smoothing of the maximum, can be clearly seen on Fig. 6b, which replicates the data shown in Fig. 6a, but for $S = 0.014$ $nm^{-1}$.
3. On a first hand, the $a_y(440)$ and $a_{CDM}(440)$ values have proven to coincide over the range of most common values (Fig. 7a); on the other hand, the $a_{CDM}(440)$ retrievals using the GSM method were validated with some success against field spectrophotometric CDOM determinations (Siegel et al., 2002). This agreement can be interpreted as an indirect quality control of $a_y$. Nevertheless, a direct validation of the $a_y(440)$ returns can profitably be attempted. The IOCCG (International Ocean Colour Coordinating Group) in situ dataset can be used for this purpose. It was prepared to test the performances of various algorithms which were proposed to retrieve the water inherent optical properties from remotely sensed ocean color data. This comparison exercise, initiated by the IOCCG, was chaired by Z.P. Lee (IOCCG, 2006) who selected in situ data (656 stations; see Fig. 2.1 in this IOCCGreport), which include simultaneous radiometric determinations (remote sensing reflectances, $R_{rs}(\lambda)$), and measurements of [Chl] and CDOM

absorption (denoted $a_g$, for gelbstoff). Time and locations needed to compute the solar zenith angle and to transform the $R_{rs}$ into $R$ (see Appendix B) are also available. The ratios $\mathbf{R}_{555}^{490}$ and $\mathbf{R}_{443}^{412}$, computed from the field $R_{rs}(\lambda)$ values at the appropriate wavelengths, are shown in Fig. 8a superimposed on the grid reproduced from Fig. 2b. Note that a considerable number of data are outside of the grid, i.e., beyond the limits which were considered as corresponding to plausible and extreme $\Phi$ values for Case 1 waters. The associated, and somewhat chaotic, histogram (Fig. 8b) shows that the most frequent $\Phi$ values are roughly centered on 2, meaning that the CDOM contents for these stations are about twice the mean oceanic values. The same kind of excess can also be observed for the NOMAD dataset (Werdell & Bailey, 2005). Actually, the NOMAD and IOCCG datasets, both extracted from NASA's archive (SeaBASS, Hooker et al., 1994; Bailey & Werdell, 2006), include Case 1 waters, but "most of the data come from locations that are relatively close to the coast" (IOCCG, 2006), which can explain the relatively high CDOM proportions.

The $a_y$ absorption coefficients, computed from the $\Phi$ values in combination with the [Chl] field values, are compared with the spectrophotometric field determinations of $a_g$ in Fig. 8c. The scatter is rather wide; actually, it is quite similar to those observed with the various inversion techniques systematically analyzed in the IOCCG report (2006). Indeed, the present RMSE (0.329, for the log-transform quantities) is similar to those published in this Report (Fig. 14.3 in this report). It is worth recalling that a robust validation is still problematic because of the difficulty in obtaining accurate $a_y$ field values in the visible part of the spectrum, and in most parts of the world ocean. Beyond the difficulty in preparing an ultra-purified water blank, the nominal accuracy of spectrophotometric determinations is anyway limiting. With an instrumental accuracy of about 0.0005 OD for the best instruments (Mueller & Fargion, 2002), and a 10 cm cell path length, the best accuracy expected for $a_y$ is 0.01 $m^{-1}$, i.e., a value about 2 to10 times larger than the most common values in the open ocean. Progress can only be expected from new techniques based, for instance, on integrating cavities or long path light guides (see e.g., Nelson et al., 2007).

4. It is not claimed that the present tool improves on other recent and more complex approaches, in particular those inter-compared in the IOCCG report (2006). Actually, it performs in a transparent way (via the grid and the lookup table) an operation similar to those, less legible, which are imbedded in minimization procedures, non-linear least-square, matrix inversion, or algebraic, techniques. It essentially has the advantage of being computationally light and in the direct continuation of classical processing methods involving band ratios, as those used to produce [Chl]. Indeed, another ratio, namely the violet-to-blue ratio, is added to derive the $\Phi$ index, then the CDM content, which allows the [Chl] estimate to be eventually corrected.

   All inversion techniques or semi-analytical algorithms, as well as the present method, include a simplified radiative transfer formulation (relating reflectance to inherent optical properties), in combination with empirical relationships, plus various hypotheses (e.g., about the slope $S$, the spectral function for backscattering coefficient, or the phytoplankton absorption…). Comparative analysis of the expected accuracy is rather difficult without resorting to a thorough end-to-end discussion of the validity of the hypotheses, the quality of the empirical relationships adopted in each method (Wang et al., 2005), in addition to the initial impact of the reflectance uncertainties (Maritorena & Siegel, 2005). Because the present method essentially rests on the MM-01 semi-analytical approach and on Eq. (1) (implicitly embedded within MM-01), its accuracy is of the same order (Morel, in press), i.e. about $\pm 30\%$ for [Chl], the $\Phi$ index, and then for $a_y$. The sensitivity of the retrieved $a_y$ value to differences between the adopted hypotheses, and the actual values of the backscattering and of the slope of the CDOM absorption, can be assessed and has been found to be rather weak.

   Anyway, the efficiency of the present method and its accuracy could be indisputably tested only if a sufficient number of $a_y$ field data of good quality and in diversified zones is available for a match up analysis. In the absence of such a validation, the overall agreement between the results of the present simple approach and of the more complex GSM inversion technique is in itself an interesting result. Indeed, the methodological differences between them are considerable, as regards the bio-optical parameterizations, the number and nature of assumptions, and ultimately the specifics of the mathematical solutions.

5. It is remarkable that the histograms for the global ocean (Figs. 3 and 6a) show that the most frequent situation corresponds to a $\Phi$ value close to unity, namely to that situation which was initially defined as being the average one and is described by Eq. (1). This is a somehow fortuitous consequence of the geographical distribution of the initial field data, which were randomly cumulated in the past (Gordon & Morel, 1983; Morel, 1988, Bricaud et al., 1998; Morel & Maritorena, 2001), and were sufficiently numerous and well distributed to be representative. These data have led to the previous mean empirical expressions from which Eq. (1)) has been derived (Morel, in press) and on which the MM-01 model rests. At regional scales, drastically differing frequency patterns, shifted from $\Phi = 1$, may recurrently occur. Among others, the Mediterranean and Pacific zones, the high latitudes in the Northern hemisphere (Figs. 2a, 5 and 6), are instances of such large and opposite anomalies.

   Another feature, rather unexpected, is the approximate log-normal character of the frequency distribution of these CDOM anomalies, for which a bio-geochemical explanation remains to be found. The range of deviations with respect to the standard situation is rather wide in Case 1 waters. Most of these deviations (about 80%), however, are comprised between a halving and a doubling of the standard CDOM value (legend Fig. 6), even if more pronounced deviations are not uncommon in open ocean. Nevertheless, the counts registered in the extreme boxes with $\Phi > 4$ (Figs. 3 and 6), generally originate from coastal Case 2 waters (not the concern of the present method). In the IOCCG and NOMAD datasets (Fig. 8b), many data, of coastal origin, also exceed this upper $\Phi$ value; in absolute values ($m^{-1}$), the corresponding $a_g$ values are largely above those of oceanic waters (compare Fig. 8c with Fig. 7a).

   If the present technique is able to detect such high $\Phi$ values, this index looses its quantitative skill when applied to Case 2 waters. Indeed, the MM-01 model which is the spine of Fig. 2 is inappropriate in such environments, so that the quantitative interpretation of the $\Phi$ values in terms of $a_y$ becomes dubious. As demonstrated by Fig. 2c, the retrieval of any $\Phi$ value is questionable in presence of very high $\Psi$ values as it happens in turbid Case 2 waters. In case of a paramount dominance of CDOM upon the optical properties (e.g., in the Baltic or the Black Sea), the grid shown in Fig. 2 is also obsolete. In such situations, the spectral reflectances become almost independent from [Chl], and this property is exploited in specialized empirical CDOM algorithms (Johannessen et al., 2003; Mannino et al., 2008).

6. As previously alluded to, the definition, and therefore the global distribution of Case 1 waters is a matter of controversy, or more properly is a question of semantics. The very definition recalled in Introduction (see also Gordon & Morel, 1983; Mobley et al., 2004) is of biogeochemical nature ("dominance of endogenous, living or detrital, organic materials"), with subsidiary, a geographical implication ("far from terrigeneous influence"). It is in no way based on rigid relationships between optical properties and [Chl], the (imperfect) index of the bulk biological activity. Conversely,

such empirical relationships are logical consequences of the definition, and when they exist and can be statistically established, they inescapably include a certain degree of natural variability around the average trends. Therefore, it is not so surprising that the relative CDOM-to-[Chl] proportions appear here to experience wide variations around the standard value. The criterion used by Lee and Hu (2006) which "allows Case 1 waters to have about a two-fold variation of non-pigment absorption… around their exact Case-1 values" actually is too restrictive when compared to what really may happen in oceanic environments. In particular, wide expanses of the oligotrophic ocean (e.g., in the Pacific Ocean) do not meet the Case-1 LH criterion, because the CDOM content is "too low", although these waters indubitably satisfy the biogeochemical definition of Case 1 waters.

## 5. Conclusion

Based on a simple idea, the semi-analytical approach here presented is efficient in discriminating the chromophoric detrital material from the algal material, by disentangling their optical effects on the radiometric quantities (reflectance) at four selected wavelengths. The present tool is straightforwardly applicable to ocean color remotely sensed data. In summary, it provides a direct estimate of a deviation index, $\Phi$, i.e., the ratio between the actual CDOM content and the "normal" content which, on average, could be expected in Case 1 waters from the local chlorophyll concentration. This index, greater or smaller than unity, denotes excess or deficit of CDOM with respect to its average, Chl-dependent, value. When knowing $\Phi$ and [Chl], the CDOM content can be expressed in terms of its absorption coefficient (at 440 nm, for instance). The initially retrieved chlorophyll concentration, [Chl], can also be re-adjusted to account for any deviation of the CDOM content with respect to its standard value. The amplitude of this readjustment, often in the range of ± 10%, can reach ± 30%, and exceptionally more (as for instance, in the Mediterranean Sea in winter, where it leads to about a halving of the initial [Chl] value).

The quantitative translation of the $\Phi$ index into $a_y$ values is no longer possible in coastal Case 2 waters, where this index, however, is available for the development of a yellow substance flag. The highest $\Phi$ values are generally detected in shallow areas ostensibly influenced by river discharges.

In open ocean and within Case 1 waters, both deficits or excesses occur. In most of the cases, these CDOM anomalies, range between about a halving and a doubling of the "normal" standard value. To the extent that the normal values (or weak excess or deficit) are the most frequent in satellite ocean color imagery, a "fair correspondence between the CDOM and the [Chl] distributions" (as quoted by Siegel, Maritorena, Nelson, & Behrenfeld, 2005) can be observed at global scale. Superimposed on this general resemblance, however, many considerable deviations occur. They exhibit seasonally and geographically well delineated patterns, which still remain to be interpreted in the light of relevant biogeochemistry and light history, probably associated with oceanic circulation, mixing process, and land–sea interactions.

## Acknowledgements

We would like to thank two anonymous reviewers for their constructive suggestions, and the GlobColour team (ACRI-ST) for the production of the merged (SeaWiFS, MERIS, and MODIS) data for the year 2006, that were used in the present study.

## Appendix A. List of acronyms

| | |
|---|---|
| CDM | Colored detrital and dissolved materials |
| CDOM | Colored dissolved organic matter |
| CZCS | Coastal zone color scanner |
| GLI | Global imager |
| GlobColour | Global Ocean Colour Project |
| IOCCG | International Ocean Colour Coordinating Group |
| MERIS | MEdium Resolution Imaging Spectrometer |
| MODIS | MODerate resolution Imaging Spectroradiometer |
| MOS | Modular Opto-electric Scanner |
| NAP | Non-algal particles (detritus, heterotrophic bacteria…) |
| NOMAD | NASA bio-Optical Marine Algorithm Data set |
| SeaBASS | SeaWiFS Bio-optical Archive and Storage System |
| SeaDAS | SeaWiFS Data Analysis System |
| SeaWiFS | Sea-viewing Wide Field-of-view Sensor |

## Appendix B. Definitions and relationships of quantities used in ocean color radiometry

The wavelength dependency is omitted, as well as dependencies on wind speed and aerosol optical thickness.

*Definitions*

*Reflectance (or Irradiance ratio)*; $R = E_u(0^-) / E_d(0^-)$ (dimensionless)

$E_u(0^-)$ and $E_d(0^-)$ are the upward and downward irradiance *beneath* the surface (at null depth, symbol $0^-$). $R$ depends on illumination conditions. It is convenient to define $R_0$, the value of $R$ when the sun is at zenith (i.e., when $\theta_s = 0$), (Fig. 7 in Morel et al., 2002). $R_j^i$ represents a ratio of irradiance reflectance ($R_0$) at the two wavelengths $i$ and $j$.

*Remote sensing reflectance*; $R_{rs} = L_w(0^+) / E_d(0^+)$ ($sr^{-1}$)

$E_d(0^+)$ is the downward irradiance (*above* the surface, symbol $0^+$); $L_w(0^+)$, actually must be written $L_w(\theta_v, \theta_s, \varphi, 0^+)$, is the water-leaving radiance, which depends on the geometry of observation, namely on the viewing angle ($\theta_v$), the solar zenith angle ($\theta_s$), and the azimuth difference ($\varphi$) between the solar plane and the plane of observation.

*Normalized water-leaving radiance*; $nL_w = F_0[L_w(0^+) / E_d(0^+)] = F_0 R_{rs}$ ($W\ m^{-2}\ sr^{-1}\ \mu m^{-1}$)

where $F_0$ is the extra-terrestrial solar irradiance, at mean Sun–Earth distance.

### A.1. Relationships

The above quantities, $nL_w$, $R_{rs}$ are corrected for the bi-directional effects (via the "$f/Q$ correction", Eq. (13.20) in Morel & Mueller, 2002). These exactly normalized quantities (superscript "ex") are related to the irradiance ratio, $R_0$ (i.e., the $R$ value when $\theta_s = 0$), through

$$R_{rs}^{ex} = R_0(\Re_0 / Q_0) \quad (A-1)$$

$$\text{and} \quad nL_w^{ex} = R_0(\Re_0 / Q_0)F_0 \quad (A-2)$$

$$\text{where} \quad R_0 = R[f_0(\theta_s = 0) / f(\theta_s)] \quad (A-3)$$

The $Q$-factor is the ratio of the upward irradiance to any upward radiance, both beneath the surface; it depends on geometry, and is expressed as

$$Q(\theta', \theta_s, \varphi) = E_u(0^-, \theta_s) / L_u(0^-, \theta', \theta'_s, \varphi) \quad (A-4)$$

$Q_0$ is the particular $Q$-value when $L_u$ is the radiance originating from nadir ($\theta' = \theta_v = 0$), and when the sun is at zenith ($\theta_s = 0$). The dimensionless factor $\Re$ merges the effect of reflection and refraction (Gordon, 2005; Wang, 2006), and $\Re_0$ (~0.529) is the particular $\Re$ value when the geometrical conditions are as above (sun at zenith, and a nadir viewing angle). $\Re_0$ is spectrally neutral and independent from the water body. The $Q_0$ factor is not spectrally neutral, so that the

computation of ratios of reflectance at two wavelengths has to be made through

$$\mathbf{R}_j^i = \left[R_0(\lambda_i)/R_0\left(\lambda_j\right)\right] = \left[R_{\mathrm{rs}}^{\mathrm{ex}}(\lambda_i)/R_{\mathrm{rs}}^{\mathrm{ex}}\left(\lambda_j\right)\right]\left[Q_0\left(\lambda_j\right)/Q_0(\lambda_i)\right]^{-1} \quad (A-5)$$

and

$$\mathbf{R}_j^i = \left[R_0(\lambda_i)/R_0\left(\lambda_j\right)\right] = \left[nL_{\mathrm{w}}^{\mathrm{ex}}(\lambda_i)/nL_{\mathrm{w}}^{\mathrm{ex}}\left(\lambda_j\right)\right]\left[Q_0\left(\lambda_j\right)/Q_0(\lambda_i)\right]^{-1}\left[F_0(\lambda_i)/F_0\left(\lambda_j\right)\right]^{-1} \quad (A-6)$$

The needed parameters ($f$, $Q$, $f/Q$) are available over the Internet using anonymous ftp, from.

oceane.obs-vlfr.fr/ pub/gentili .

The tables corresponding to the grid in Fig. 2b are available at

ftp://oceane.obs-vlfr.fr/ pub/gentili/CDM-index-Table.interpol

ftp://oceane.obs-vlfr.fr/ pub/gentili/Chl-R490:R555-Table.interpol

These two tables cover the grid shown in Fig. 2b within the same limits. With the $\mathbf{R}_{443}^{412}$ and $\mathbf{R}_{555}^{490}$ ratios, used as inputs, the first table provides the $\Phi$ index, and the second Table the [Chl] value. When the input values fall outside of the grid of Fig. 2b, the $\Phi$ index and the [Chl] value cannot be retrieved.

## References


Bailey, S. W., & Werdell, P. J. (2006). A multi-sensor approach for the on-orbit validation of ocean color satellite data products. *Remote Sensing of Environment*, *102*, 12−23.

Bricaud, A., Morel, A., Babin, M., Allali, K., & Claustre, H. (1998). Variations of light absorption by suspended particles with chlorophyll a concentration in oceanic (case 1) waters: Analysis and implications for bio-optical models. *Journal of Geophysical Research-Oceans*, *103*, 31033−31044.

Bricaud, A., Morel, A., & Prieur, L. (1981). Absorption by dissolved organic matter of the sea (yellow substance) in the UV and visible domains. *Limnology and Oceanography*, *26*, 43−53.

Brown, C. A., Huot, Y., Werdell, P. J., Gentili, B., & Claustre, H. (2008). The origin and global distribution of second order variability in satellite ocean color and its potential applications to algorithm development. *Remote Sensing of Environment*, *112*, 4186−4203. doi:10.1016/j.rse.2008.06.008.

Carder, K. L., Chen, F. C., Lee, Z. P., Hawes, S. K., & Kamykowski, D. (1999). Semianalytic Moderate Resolution Imaging Spectrometer algorithms for chlorophyll-a and absorption with bio-optical domains based on nitrate-depletion temperatures. *Journal of Geophysical Research*, *104*, 5403−5421.

Garver, S. A., & Siegel, D. A. (1997). Inherent optical property inversion of ocean color spectra and its biogeochemical interpretation. 1. Time series from the Sargasso Sea. *Journal of Geophysical Research*, *102*, 18607−18625.

Gordon, H. R. (2005). Normalized water-leaving radiance: Revisiting the influence of surface roughness. *Applied Optics*, *44*, 241−248.

Gordon, H. R., & Morel, A. (1983). *Remote sensing of ocean color for interpretation of satellite visible imagery*, *Vol. 114*. (pp. )New York, Berlin, Heidelberg, Tokyo: Springer Verlag.

Hoge, F. E., & Lyon, P. E. (1996). Satellite retrieval of inherent optical properties by linear matrix inversion of oceanic radiance models: An analysis of model and radiance measurement errors. *Journal of Geophysical Research*, *101*, 16631−16648.

Hooker, S.B., McClain, C.R., Firestone, E.R., Westphal, T.L., Yeh, E.N., & Geo, Y., (1994). The SeaWiFS Bio-optical Archive and Storage System (SeaBASS),Part 1. NASA Technical Memo. 104566, 20, 37.

IOCCG (2006). Remote sensing of inherent optical properties: Fundamentals, tests of algorithms and applications. Report Number 5. In V. Stuart (Ed.), *Reports of the International Ocean-Colour Coordinating Group* (pp. 1−126). Dartmouth, Nova Scotia, Canada.

Johannessen, S. C., Miller, W. L., & Cullen, J. J. (2003). Calculation of UV attenuation and colored dissolved organic matter absorption spectra from measurements of ocean color. *Journal of Geophysical Research*, *108*. doi:10.1029/2000JC000514.

Lee, Z. P., Carder, K. L., & Arnone, R. (2002). Deriving inherent optical properties from water color: A multi-band quasi-analytical algorithm for optically deep waters. *Applied Optics*, *41*, 5755−5772.

Lee, Z. P., & Hu, C. (2006). Global distribution of Case-1 waters: An analysis from SeaWiFS measurements. *Remote Sensing of Environment*, *101*, 270−276.

Mannino, A., Russ, M. E., & Hooker, S. B. (2008). Algorithm development and validation for satellite-derived distributions of DOC and CDOM in the U.S. Middle Atlantic Bight. *Journal of Geophysical Research*, *113*. doi:10.1029/2007JC004493.

Maritorena, S., & Siegel, D. A. (2005). Consistent merging of satellite ocean color data sets using a bio-optical model. *Remote Sensing of Environment*, *94*, 429−440.

Maritorena, S., Siegel, D. A., & Peterson, A. (2002). Optimization of a semi-analytical ocean color model for global applications. *Applied Optics*, *41*, 2705−2714.

Mobley, C. D., Stramski, D., Bissett, W. P., & Boss, E. (2004). Optical modeling of ocean waters: Is the Case 1–Case 2 classification still useful? *Oceanography*, *17*, 61−67.

Morel, A. (1980). In-water and remote measurements of ocean color. *Boundary Layer Meteorology*, *18*, 177−201.

Morel, A. (1988). Optical modeling of the upper ocean in relation to its biogenous matter content. *Journal of Geophysical Research*, *93*, 10749−10768.

Morel, A., (in press). Are the empirical relationships describing the bio-optical properties of Case 1 waters consistent and internally compatible? Journal of Geophysical Research, 114. doi:10.1029/2008JC004803.

Morel, A., Antoine, D., & Gentili, B. (2002). Bidirectional reflectance of oceanic waters: Accounting for Raman emission and varying particle scattering phase function. *Applied Optics*, *41*, 6289−6306.

Morel, A., & Bélanger, S. (2006). Improved detection of turbid waters from ocean color sensors information. *Remote Sensing of Environment*, *102*, 237−249.

Morel, A., Claustre, H., Antoine, D., & Gentili, B. (2007). Natural variability of bio-optical properties in Case 1 waters: Attenuation and reflectance within the visible and near-UV spectral domains as observed in South Pacific and Mediterranean waters. *Biogeosciences*, *4*, 2147−2178.

Morel, A., & Gentili, B. (1991). Diffuse reflectance of oceanic waters — Its dependence on sun angle as influenced by the molecular-scattering contribution. *Applied Optics*, *30*, 4427−4438.

Morel, A., & Gordon, H. R. (1980). Report of the working group on water color. *Boundary Layer Meteorology*, *18*, 343−355.

Morel, A., Gentili, B., Claustre, H., Babin, M., Bricaud, A., Ras, J., et al. (2007). Optical properties of the "clearest" natural waters. *Limnology and Oceanography*, *52*, 217−229.

Morel, A., Huot, Y., Gentili, B., Werdell, P. J., Hooker, S. B., & Franz, B. A. (2007). Examining the consistency of products derived from various ocean color sensors in open ocean (Case 1) waters in the perspective of a multi-sensor approach. *Remote Sensing of Environment*, *111*, 69−88.

Morel, A., & Maritorena, S. (2001). Bio-optical properties of oceanic waters: A reappraisal. *Journal of Geophysical Research-Oceans*, *106*, 7163−7180.

Morel, A., & Mueller, J. L. (2002). Normalized water-leaving radiance and remote sensing reflectance: Bidirectional reflectance and other factors. *Ocean Optics Protocols for satellite ocean color sensor validation, NASA/TM-2002-210004/Rev3-Vol2* (pp.183−210).

Mueller, J. L., & Fargion, G. S. (2002). Ocean Optics Protocols for satellite ocean color sensor validation, revision 3. 308 pp. *NASA /Technical Memo.-2002-210004/Rev3-vol1,vol2*.

Nelson, N. B., Siegel, D. A., Carlson, C. A., Swan, C., Smethie, W. M., Jr., & Khatiwala, S. (2007). Hydrography of chromophoric dissolved organic matter in the North Atlantic. *Deep-Sea Research I*, *54*, 710−731.

Nelson, N. B., Siegel, D. A., & Michaels, A. F. (1998). Seasonal dynamics of colored dissolved material in the Sargasso Sea. *Deep-Sea Research I*, *45*, 931−957.

O'Reilly, J. E., Maritorena, S., Mitchell, B. G., Siegel, D. A., Carder, K. L., Garver, A., et al. (1998). Ocean color algorithms for SeaWiFS. *Journal of Geophysical Research*, *103*, 24937−24953.

O'Reilly, J. E., Maritorena, S., Siegel, D. A., O'Brien, M. C., Toole, D., Mitchell, B. G., et al. (2000). Ocean color chlorophyll a algorithms for SeaWiFS, OC2, and OC4: version 4. *SeaWiFS postlaunch calibration and validation analyses, Part 3NASA/TM 206892*, *Vol. 11*. (pp. 9−23).

Schiller, H., & Doerffer, R. (2005). Improved determination of coastal water constituent concentrations from MERIS data. *IEEE Transactions on Geoscience and Remote Sensing*, *43*, 1585−1591.

Siegel, D. A., Maritorena, S., Nelson, N. B., & Behrenfeld, M. J. (2005). Independence and interdependencies of global ocean color properties: Re-assessing the bio-optical assumption. *Journal of Geophysical Research*, *110*, C07011. doi:10.1029/2004JC002527.

Siegel, D. A., Maritorena, S., Nelson, N. B., Behrenfeld, M. J., & McClain, C. R. (2005). Colored dissolved organic matter and its influence on the satellite-based charaterization of the ocean biosphere. *Geophysical Research Letters*, *32*, L20605. doi:10.1029/2005GL024310.

Siegel, D. A., Maritorena, S., Nelson, N. B., Hansell, D. A., & Lorenzi-Kaiser, M. (2002). Global distribution and dynamics of colored dissolved and detrital organic materials. *Journal of Geophysical Research*, *107*(C12), 3228. doi:10,1029/2001JC000965.

Smyth, T. J., Moore, G. F., Hirata, T., & Aiken, J. (2006). Semianalytical model for the derivation of ocean color inherent optical properties: Description, implementation, and performance assessment. *Applied Optics*, *45*, 8116−8131.

Wang, M. (2006). Effects of ocean surface reflectance variation with solar elevation on normalized water-leaving radiance. *Applied Optics*, *45*, 4122−4128.

Wang, P., Boss, E., & Roesler, C. (2005). Uncertainties of inherent optical properties obtained from semi-analytical inversions of ocean color. *Applied Optics*, *44*, 4074−4085.

Werdell, P. J., & Bailey, S. W. (2005). An improved in-situ bio-optical data set for ocean color algorithm development and satellite data product validation. *Remote Sensing of Environment*, *98*, 122−140.